*Int. J. Electrochem. Sci.*, 15 **(2020)** 6165 – 6176, doi: 10.20964/2020.07.02

International Journal of
ELECTROCHEMICAL
SCIENCE
www.electrochemsci.org

*Short Communication*

# Microstructure and Corrosion behavior of the Dy-doped sintered Nd-Fe-B Magnets Processed by Low-temperature Heat Treatment

*Qing-Xian Hu[1], Xiao-Li Wang[1,*], Yan-Xin Qiao[1], Fu-Gang Chen[1], Kai-Hong Ding[2], Zong-Jie Peng[2], Yong-Cong Sun[2], Mu-Sen Li[3]*

[1] National Demonstration Center for Experimental Materials Science and Engineering Education (Jiangsu University of Science and Technology), Zhenjiang, 212003, China
[2] Yantai Shou-gang Magnetic Materials Inc. Yantai 265500, China
[3] Key Laboratory for Liquid-Solid Structural Evolution and Processing of Materials (Ministry of Education), Shandong University, Jinan Shandong 250061, China
[*]E-mail: happysmile555@yeah.net

*Received:* 10 October 2019 / *Accepted:* 3 January 2020 / *Published:* 10 June 2020

The low-temperature heat treatment process can be used to replace the traditional two-stage heat treatment process during the production of the Dy-doped Nd-Fe-B magnets, which saves the energy and also shortens the production period. In this work, the microstructure and corrosion behaviors of Nd-Fe-B magnets doped with Dy were analyzed by the scanning electron microscope observation, electrochemical and mass loss test. The results indicated that the corrosion resistance of the magnet with one-stage low-temperature annealing process was better than that with two-stage annealing process. Lots of (Pr, Nd, Dy)-oxide and Dy-oxide formed on the surface of the magnets after one-stage low-temperature annealing process, which decreased the electrode potential differences between the main phase grains and these oxide particles, and this further reduced the corrosion reaction driving force of the magnets.

**Keywords:** Nd-Fe-B magnets doped with Dy, Low-temperature process, Corrosion resistance

## 1. INTRODUCTION

Because of outstanding magnetic properties such as high magnetic energy product and high coercivity Nd-Fe-B magnets have received many investigations in the last few decades. Most of them focused on how to improve the coercivity [1-6] and the corrosion resistance by doping with different elements [7-9]. Some investigations are also carried out to improve the corrosion resistance of the Nd-Fe-B through various coating technologies [10-12]. However, few studies were performed to reveal

the effect mechanism of different annealing processing on the corrosion behavior of the Dy-doped Nd-Fe-B magnets. Our previous studies showed that the magnetic and mechanical properties of the Dy-doped sintered Nd-Fe-B magnets after the one-stage low-temperature annealing process at 400-600℃ for 2 h were basically the same as the ones heat treated by two-stage process consisting of 800-900 °C × 2h and 400-600 °C × 2h [13-15]. The corrosion behavior of these Nd-Fe-B magnets has not been well studied. The present study further compared the microstructure and the corrosion behavior of Nd-Fe-B magnets with the two different heat treatment processes.

As one knows that the two-stage annealing process is widely applied during the preparations of Nd-Fe-B magnets doped with Dy. This method has the certain drawbacks such as high energy-consumption and low fabrication efficiency. In order to study the possibility that the traditional two-stage annealing process can be replaced by the one-stage low-temperature annealing process, it was necessary to further study the difference of the microstructure and corrosion resistance between the magnets with different annealing processes. In this paper, the different microstructure and the corrosion resistance between the Dy-doped Nd-Fe-B magnet with one-stage low-temperature annealing process and the one by two-stage annealing process were analyzed, and the mechanism about the different corrosion resistance was discussed.

## 2. EXPERIMENTAL

### *2.1. The experimental materials*

The composition of these magnets was shown in Table 1. The detailed preparation technique of the Nd-Fe-B magnets has been described in our previous paper [14]. Dy-doped sintered Nd-Fe-B magnets with one-stage annealing process of 400-600 °C for 2h (namely, low-temperature process) had almost the same magnetic properties as the ones by the heat treatment process of 800-900 °C for 2h and 400-600 °C for 2h (namely, two-stage process).

**Table 1**. Composition of the sintered NdFeB magnets（wt%）doped with Dy

| Elements | Nd | Pr | Dy | Co | B | Cu | Al | Fe |
|---|---|---|---|---|---|---|---|---|
| wt (%) | 21.32 | 5.33 | 4.35 | 0.9 | 1.07 | 0.01 | 0.01 | Bal. |

The microstructure of the magnets was characterized using the optical microscope and scanning electron microscope (SEM) equiped with an energy dispersive X-ray spectrometer (EDS, SU-70 model made in Japan).

Electrochemical corrosion behaviors of the two tested samples were conducted in 3.5 wt % NaCl solution at 25 °C ± 1 °C. The 3.5 wt.% NaCl solution was prepared using analytical-grade sodium chloride and distilled water. The electrochemical behaviors of the tested alloys were obtained using a CHI660E (Shanghai Chenhua Instruments Corp., Ltd. Shanghai, China) electrochemical workstation and a three-electrode electrochemical cell, and the method was described in the literature [16]. Potentiodynamic polarization was performed at a scan rate of 0.333 mV/s from −500m$V_{SCE}$ below the open circuit potential (OCP) and terminated when the current density reached to 100 mA/$cm^2$. All

measurements were repeated at least three times in naturally-aerated 3.5 wt.% NaCl solution without stirring to ensure the reproducibility. View software was used to fit the electrochemical data.

The mass loss tests were conducted using an environmental test chambers (EHS-221, ESPAC instrument and Analysis Company, Japan). The sample was a small cylinder, and three magnet samples were taken for each state. Prior to the experiment, the samples were gradually ground with SiC papers down to 1200 grit, polished with a diamond paste of 0.1 μm, then cleaned in ethanol, and finally dried with hot air. The corresponding surface area was calculated, and the mass was weighed by electronic balance, and then put into the test chamber for experiment. The temperature and the relative humidity were 120 ℃ and 100%, respectively. Prior to the mass loss tests, the weight of the sample was weighted and recorded for $m_0$. The samples were taken out every 48 hours and the total teste time is 480 h. Five specimens were taken for this experiment from two states of magnets, respectively. The mass loss rates of the two tested samples after each interval of immersion were calculated based on the mass loss, $\Delta m$, using Equation (1) shown as following:

$$\Delta m = \frac{m_0 - m_1}{S \times t} \quad (1)$$

where $m_0$ is the weight (mg) of the sample before the corrosion test, $m_1$ is the weight (mg) of the sample after the corrosion test, $S$ is the surface area of the sample ($cm^2$), and $t$ is the immersion time.

## 3. RESULTS AND DISCUSSION

### *3.1 Microstructure observations*

Figure 1 shows the optical microscope images of the as-sintered Nd-Fe-B magnet without annealing (Figure 1(a)), the magnet after two-stage annealing process (Figure 1(b)) and the magnet after one-stage annealing process (Figure 1(c)). Three colors (light, black and grey) can be observed in Figure 1, which corresponds to the main phase $Nd_2Fe_{14}B$ grains, the grain boundary Nd/B-rich phase and poles, respectively. In Figure 1(a) it can be seen that the grain boundaries of the matrix phase were not clear, and the Nd-rich phase on grain boundaries was unevenly distributed, mainly gathering at the $Nd_2Fe_{14}B$ corners. This results in a strong magnetic exchange coupling effect among the $Nd_2Fe_{14}B$ phase grains. Therefore, the coercivity of as-sintered magnets was low. From the Figure 1 (b) and (c), it can be seen that the grain boundaries were very clear. The Nd rich phase was evenly distributed on the grain boundaries, which was advantageous to increase the coercivity of the magnets because it made magnetic exchange coupling effect among the matrix phase grains reduce. Compared to the grains of the magnets after heat treatment with the low-temperature process, the grains of the magnets after heat treatment with the two-stage process were fine. The increased grain boundaries induced by grain refinement provided more channels for corrosion, which caused the corrosion resistance degradation. However, the grain size of the magnets after heat treatment with low-temperature process was bigger and there were a lot of sediment on grain surface, which caused the increase of surface roughness. Grain boundaries, precipitation phases and the surface roughness played the role of separation of main grains, weakness the static magnetic coupling of adjacent grains and pinning domain wall, which can improve the magnet coercivity [17].

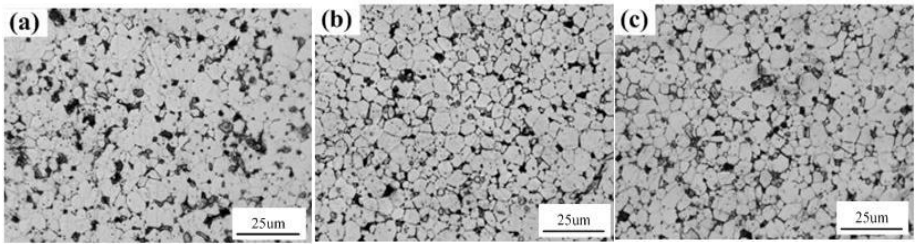


**Figure 1.** Metallographic images of (a) as-sintered (b) two-stage process and (c) Nd-Fe-B magnet after low-temperature process

*3.2 SEM observation and EDS analysis*

From Table 2, it can been seen that Dy content of the magnets after heat treatment with two-stage process on the grain boundary phase, in the main phase grain boundaries and the interior of grains was 1.62 wt %, 5.42 wt % and 4.23 % , respectively. Obviously, Dy elements gathered in the main phase. The content of Pr and Nd on the grain boundaries of the main crystal phase was 21.66 wt %, which was lower than the ones inside the main grains. This is because some of Pr and Nd elements were replaced by Dy element in the main crystal phase grains, which formed (Pr, Nd, Dy) $_2Fe_{14}B$ hard magnetic shell with high magneto crystalline anisotropy field, and at the same time, Nd element in main phase was replaced by Dy element which formed $(Nd, Dy)_2Fe_{14}B$. As a result, the intrinsic coercivity of magnets was improved. The two-stage process provided enough dynamics condition for Dy element diffusion, and the liquid Pr/Nd-rich phase at high temperature provided diffusion paths for Dy. Al and Cu elements increase the wetting ability of the grain boundary phase that made Dy element diffuse from the corner of grain boundaries to the grain boundaries of the main phase and further into the main crystal phase.

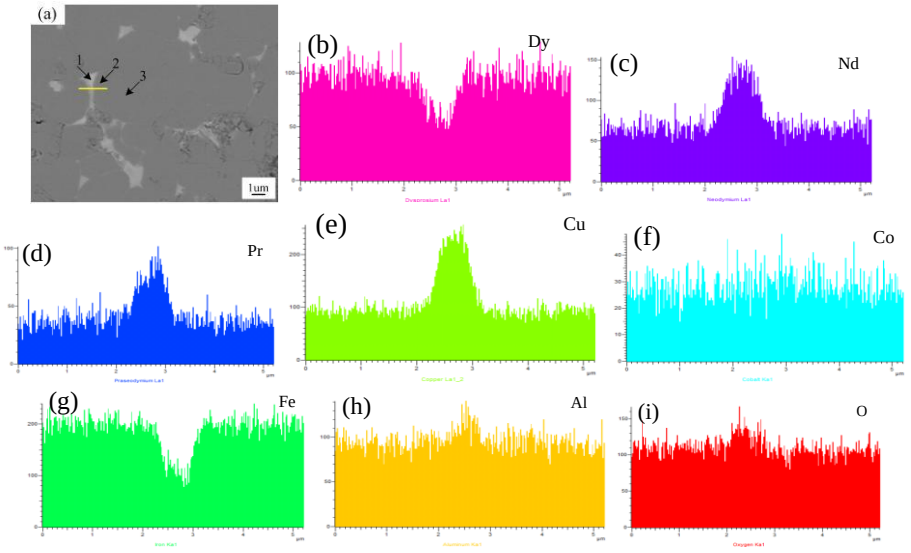


**Figure 2.** Element distribution on grain boundary phase, the interface between the main crystal phase and inner main grain phase of NdFeB magnets doped with Dy and heat treatment by two-stage process

**Table 2.** Compositions of the triple junctions (1), interface of the main crystal phase (2) and inner main phase grains (3) of two-stage NdFeB magnets doped with Dy (wt%)

| Position | Nd | Pr | Dy | Fe | Al | Cu | Co | O |
|---|---|---|---|---|---|---|---|---|
| 1 | 40.71 | 14.95 | 1.62 | 32.96 | 1.35 | / | 6.83 | 1.59 |
| 2 | 17.37 | 4.29 | 5.42 | 68.86 | 0.75 | 0.02 | 2.47 | 0.82 |
| 3 | 17.78 | 4.28 | 4.23 | 69.69 | 0.84 | 0.40 | 2.05 | 0.74 |

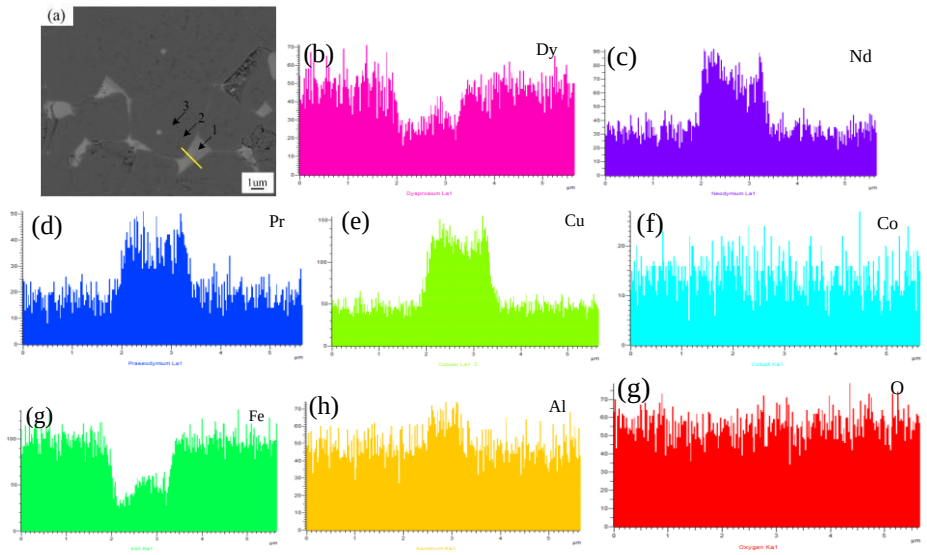


**Figure 3.** Element distribution on grain boundary phase, the interface between the main crystal phase and inner main grain phase of the NdFeB magnets doped with Dy and heat treatment by low-temperature process

**Table 3.** Compositions of the triple junctions (1), interface of the main crystal phase (2) and inner main phase grains (3) of the NdFeB magnets doped with Dy (wt %) and heat treatment by low-temperature process

| Position | Nd | Pr | Dy | Fe | Al | Cu | Co | O |
|---|---|---|---|---|---|---|---|---|
| 1 | 40.14 | 12.74 | 1.75 | 35.21 | 1.52 | / | 7.11 | 1.53 |
| 2 | 15.99 | 3.41 | 5.91 | 70.72 | 0.74 | / | 2.18 | 1.04 |
| 3 | 17.59 | 3.11 | 0.91 | 73.53 | 0.78 | / | 3.10 | 0.97 |

From Table 3, it can been seen that Dy element contents of low-temperature heat treatment magnets on the grain boundary phase, in the grain boundaries of the main phase and the interior of the grains was 1.75 wt%, 5.91 wt% and 0.91% , respectively. Compared to the magnets with two-stage heat treatment process, the Dy element tends to gather in the grain boundaries of the main crystal phase. This special Dy-rich shell structure can decrease magnetic dilution that caused by antiferromagnetic coupling between Dy atoms and Fe atoms, and avoid the negative impact on the magnetization. It revealed that the distribution of Dy elements in the magnets with low-temperature process was more reasonable than in the ones with two-stage process. At the same time, the content of

Pr and Nd on the main phase grain boundary was 19.3 wt %, which was lower than that inside grains (20.7 wt %). It was illustrated that part of Pr and Nd was replaced by Dy element on the main grain boundary, which formed (Pr, Nd, Dy) $_2$ $Fe_{14}B$ phase. Hence, there was a layer of hard magnetic phase on the grain boundary of the main crystal phase about the magnets after heat treatment with low-temperature process. Cu was not detected in the corresponding point scanning because the amount of Cu was little and its distribution was uneven on grain boundary.

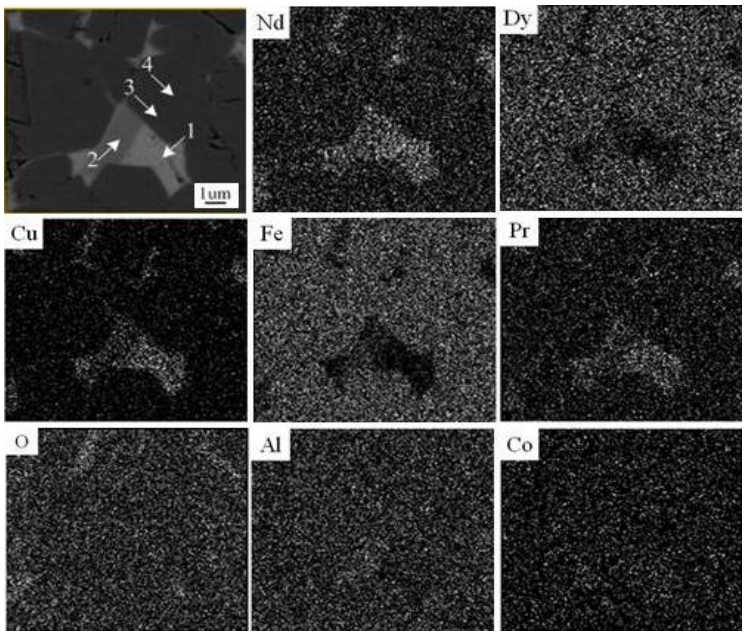


**Figure 4.** Distribution of the elements in the triple junctions and the main crystal phase of the magnets heat treatment by low-temperature process

**Table 4.** Composition of the triple junctions (1,2) , surface region of the main crystal phase (3) and inner main phase grains (4) of the NdFeB magnets doped with Dy (wt %) and heat treatment by low-temperature process

| Position | Nd | Pr | Dy | Fe | Al | Cu | Co | O |
|---|---|---|---|---|---|---|---|---|
| 1 | 55.18 | 21.43 | 2.48 | 3.33 | 0.22 | 1.59 | 14.27 | 1.50 |
| 2 | 40.31 | 14.28 | 1.12 | 35.30 | 0.74 | 1.61 | 5.89 | 1.48 |
| 3 | 18.05 | 3.96 | 5.35 | 70.64 | 0.82 | / | 0.32 | 0.86 |
| 4 | 16.95 | 3.92 | 5.95 | 70.30 | 0.89 | / | 1.03 | 0.96 |

In order to study the distribution of Cu element in the magnets after heat treatment with low-temperature process, further analysis was carried out in Figure 4. The result was shown that in Figure 4 and Table 4. The position 1 was relatively brighter than the position 2. It can be seen that the content of Pr and Nd at position 1 was 76.61 wt %, which was more than the one at position 2 that was 54.59 wt %. The content of Co was 14.27% at position 1, which was much higher than 0.9 wt % that was added into the magnets. The content of Dy and O was also higher than the one at position 2. It was showed that the elements on the grain boundary phase were not uniform. According to the results of

map scanning and the point scanning analysis of the position 1 and 2, the content of Pr and Nd between position 1 and 2 varied wildly but the difference of O content was not big. It can be deduced that it was not O element that caused the different contrast area of the grain boundary phase. It was different with the research results of Li [18]. W. F. Li thought the contrast of the grain boundary phase was different because of the different O content. In combination with the surface scanning results analysis, Cu element mainly distributed in the corner area of the grain boundary of Pr, Nd and Co but its distribution at the corner area of the grain boundary was not uniform. Cu element was not on the grain boundary of the main crystal phase and the internal main phase grain. A small amount of Cu was added into the NdFeB magnets doped with Dy and it can effectively reduce the eutectic temperature of the rare earth phase on the grain boundary [19]. Therefore, the distribution of the grain boundary phase of the magnets was improved and formed a continuous thin layer on the grain boundaries by low-temperature heat treatment process. At the corner of grain boundary where gathered rich (Pr, Nd, Co), the content of Dy was more on the main grain boundary and inside main grain than the one at the corner of grain boundary.

Through the above analysis, Dy element diffused from the grain boundary to the main phase grain boundary and formed hard-magnetized thin layer structure that was beneficial to improve the coercivity. Part of Cu and Al with low melting points dissolved into the main crystal phase, or distributed on grain boundary phase that changed the grain boundary eutectic transformation temperature of Nd rich phase. The wettability between the grain boundary phase and the main crystal phase was improved by low melting eutectic phase. The demagnetization exchange coupling effect among the main crystal phase was enhanced, and the coercivity was increased. Co element gathered at the corners. Moneim and Camp investigated the corrosion behavior of the magnets doped with Co and found that Co can lead to the formation of (Nd, Co) intermetallic compound or Co bearing $Nd_3O$ phase. It improved the corrosion resistance of rare earth phase on the grain boundary so that the corrosion resistance of the magnets was improved [20, 21].

### *3.3 Back scattered electron observation*

Figure 5 compared the microstructure of the magnets after heat treatment with two-stage process and the one after heat treatment only with low-temperature process. Both small particles (~100 nm) and big particles (~1 μm) can be seen on the surface of the magnet after heat treatment with low-temperature process. However there were not such particles on the surface of the magnet after heat treatment with two-stage process. EDS results were shown in Table 5. It showed that there were three kinds of particles: (Pr, Nd, Dy)-rich oxide particles, (Dy, Cu)-rich particles, and Dy-rich oxide particles. Particles with the size about 1 μm were mainly (Pr, Nd, Dy)-rich oxide particles. The electrode potential difference between (Pr, Nd, Dy)-rich oxide particles and Dy-rich oxide particles was reduced because of the higher electrode potential of (Pr, Nd, Dy)-rich oxide particles and Dy-rich oxide particles, which decreased the corrosion reaction driving force of magnets. Therefore, the corrosion resistance of the magnets after heat treatment with one-step low-temperature process was superior to the ones after heat treatment with two-stage process.

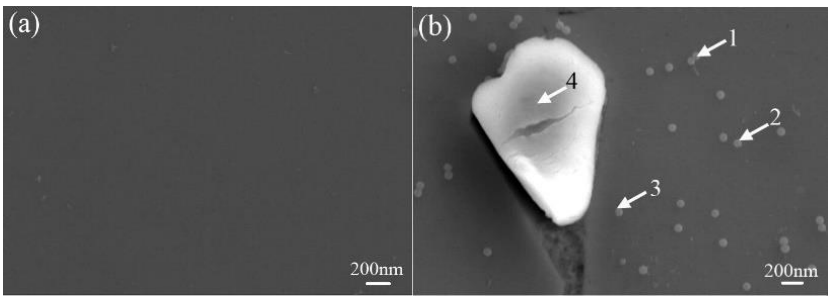


**Figure 5.** SEM images of the two tested samples (a) two-stage process and (b) low-temperature process

**Table 5.** Composition of the particles on the surface of the magnets in Figure 5(b) (wt %)

| Position | Nd | Pr | Dy | Fe | Al | Cu | Co | O |
|---|---|---|---|---|---|---|---|---|
| 1 | / | / | 47.57 | 33.95 | 0.48 | 18.00 | / | / |
| 2 | 52.50 | 13.16 | 11.05 | / | 0.04 | / | / | 22.25 |
| 3 | 16.70 | 4.29 | 6.26 | 67.77 | 0.74 | 0.18 | 3.21 | 0.85 |
| 4 | 47.58 | 12.68 | 9.54 | 5.64 | 0.05 | / | / | 24.52 |

*3.4 Electrochemical behavior*

The corrosion potential of the Nd-Fe-B magnets in 3.5 wt % NaCl solution was shown in Figure 6. It can be seen that the two magnets gradually reached a steady state of -0.81 $V_{SCE}$ and -0.845 $V_{SCE}$ for low-temperature ageing magnets and two-stage ageing magnets respectively. Therefore, the corrosion behavior of low-temperature annealing magnet is similar to that of two-stage annealing magnets.

Potentiodynamic polarization curves of two tested samples in 3.5 wt % NaCl solution was shown in Figure 7. It is seen from Figure 7 that both samples exhibited active dissolution, and no sigh of passivation was observed. The corrosion current density ($i_{corr}$) for the two-stage processed sample and low temperature aged sample was $6.81 \times 10^{-6}$ A·cm$^{-2}$ and $3.54 \times 10^{-6}$ A·cm$^{-2}$, respectively. The lower $E_{corr}$ and higher $i_{corr}$ of the two-stage processed sample suggested that the low temperature aged sample had a superior corrosion resistance [22].

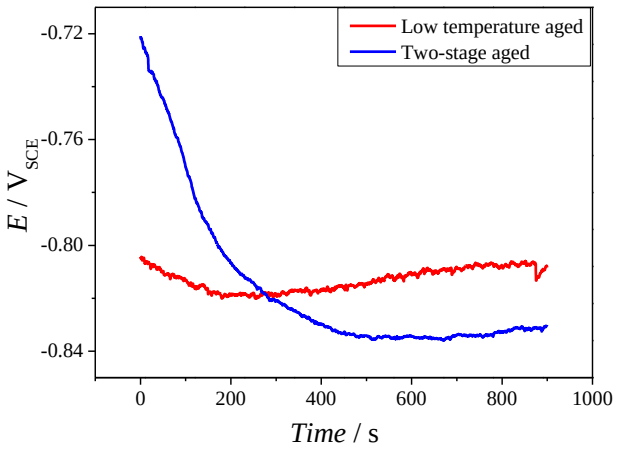


**Figure 6.** Corrosion potential of the two tested samples in 3.5wt% NaCl solution.

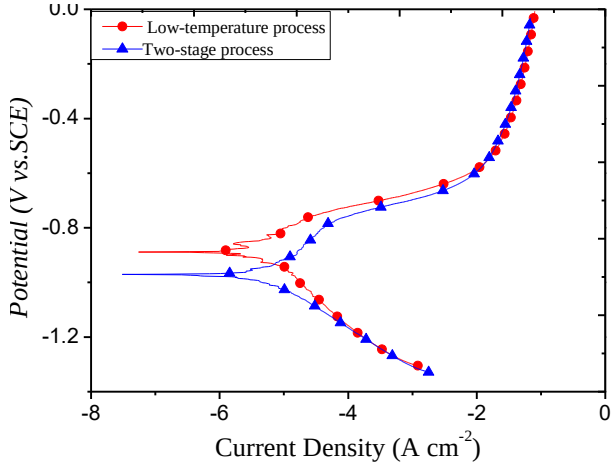


**Figure 7.** Potentiodynamic polarization curves of the two tested samples in 3.5wt% NaCl solution

**Table 6.** Electrochemical parameters of the two tested samples

| | $E_{corr}$ ($V_{SCE}$) | $I_{corr}$ (A/cm$^2$) |
|---|---|---|
| Two-stage process | -0.97 | $6.81\times10^{-6}$ |
| Low-temperature process | -0.89 | $3.5\times10^{-6}$ |

There were many factors affecting the electrochemical corrosion of NdFeB magnets, such as the corrosion potential difference between precipitated Nd rich phase at grain boundaries and the matrix $Nd_2Fe_{14}B$ phase, grain size and magnet density, etc. Nevertheless, the key factor was the corrosion potential between the Nd rich phase and the matrix $Nd_2Fe_{14}B$ phase. The greater the potential difference, the easier to corrosion. The intention of aging treatment was to improve the distribution homogeneity of Nd-rich phase, so as to decrease the coupling between neighbouring grains and then increase the coercivity. However, the results showed that the rich Nd phase distributed in thin layer

form might be one of the main reasons that decreases the corrosion resistance, and this will be further examined in future. At the same time, more grain boundaries appeared in the two-stage aged magnets, which was also one of the key factors that resulted in the worse corrosion resistance.

*3.5* Mass loss test

Accelerating weight loss method was adapted to characterize oxidation corrosion [23]. In order to quantitatively evaluate the corrosion resistance of the magnets by low-temperature heat treatment and the ones by two-stage heat treatment, mass loss test was carried out for these two kinds of samples.

The color of samples was shiny silver prior to the mass loss test and then turned to blue-black after 480 hours. The existence of pulverization was on the surface of the tested samples after mass loss test. It was found that the oxygen content on the surface of the magnets was increased after the mass loss testing. It can be preliminary inferred that the appearance of the blue-black corrosion products resulted from the corrosion of samples. Figure 8 showed the mass loss rate curves of the two tested samples vs CE time. Two plateaus of no mass loss appeared in the mass loss rate curve. The mass loss rate linearly increased with immersion time when the immersion time was less than 96 h. This phenomenon is in good agreement with the result of potentiodynamic polarization test indicating the tested samples in the state of active dissolution [24-26]. Then the first plateaus appeared when the immersion time prolonged to 192 h. In this stage, the mass loss rates of samples were no longer changed and maintain stable. This may be the formation a layer of compact and chemically stable oxide film that spontaneously covers the metal surface which is mainly composed of Boron-containing [27]. According to the published literature [28], the reaction between the Nd-riched grains and water vapor can induce the generation of H atoms. The reaction between the H atoms and the Nd rich phase would lead to the generated $Nd_3H$. The generation of $Nd_3H$ can induce the volume expansion of grain boundary which eventually leaded to the fracture of grain boundary. This would lead to the increasing of mass loss rate when the mass loss test time prolong to 192 h.

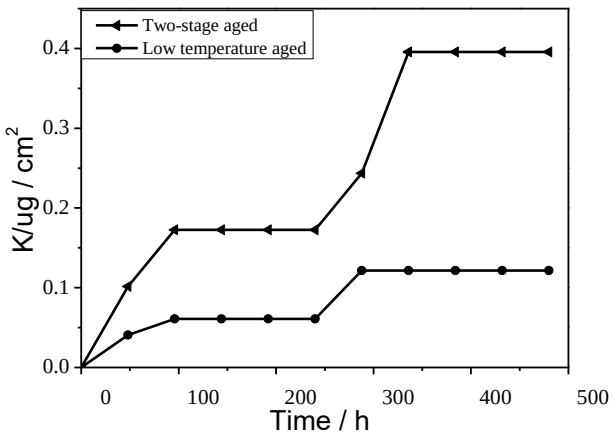


**Figure 8.** The mass loss curve of the two tested samples vs CE time

## 4. CONCLUSION

The electrochemical corrosion behavior showed that the two tested samples were dominant by anodic dissolution in 3.5 % NaCl solution. The mass loss test result was consistent with the electrochemical behavior. This indicated that the low-temperature processed sample has superior corrosion resistance. Because of the existence of (Pr, Nd, Dy) oxides and Dy oxide in the magnets by low-temperature heat treatment, the main crystal phase electrode potential difference was decreased, and then the corrosion reaction driving force of the magnets was reduced. Therefore, the corrosion resistance of the magnets by low-temperature heat treatment was superior to the ones by two-stage heat treatment.

ACKNOWLEDGMENT
This work is supported by Natural Science Foundation of Jiangsu Province (No. BK20190975)

## References

1. T.T. Sasaki, Y. Takada, H. Okazaki, T. Ohkubo, T. Nakamura, T. Sato, A. Kato, Y. Kaneko and K. Hono, *J. Alloys Compd*., 790 (2019) 750.
2. J.J. Li, C.J. Guo, T.J. Zhou, Z.Q. Qi, X. Yu, B. Yang and M.G. Zhu, *J. Magn. Magn. Mater*., 454 (2018) 215.
3. Y.L. Lee, Y.J. Wang, H.W. Chang and W.C. Chang, *J. Magn. Magn. Mater*., 478 (2019) 43.
4. H.W. Chang, Y.I. Lee, P.H. Liao and W.C. Chang, *Scripta Mater*., 146 (2018) 222.
5. L. Liu, H. Sepehri-Amin, T. Ohkubo, M. Yano, A. Kato, T. Shoji and K. Hono, *J. Alloys Compd*., 666 (2016) 432.
6. F.G. Chen, M.Q. Cong, H.M. Chen, N. Liu, D. P. Wang, X.L. Wang, Y. Zhao and W.Q. Zhao, *J. Alloys Compd.,* DOI:10.1016/j.jallcom.2019.152965.
7. J.H. Feng, H. Zhou, D.Y. Chen, T. Bian, A.H. Yuan, *Electrochim. Acta*, 331 (2020) 135445.
8. W. Jiang, L.D. Shen, K. Wang, M.Y. Xu and Z.J. Tian, *J. Alloys Compd*., 787 (2019) 1089.
9. S. Pavón, A. Fortuny, M.T. Coll, A.M. Sastre, *J. Magn. Magn. Mater*., 222 (2018) 359.
10. Y.Q. Huang, H.Q. Li, M. Zuo, L. Tao, W. Wang, J. Zhang, Q. Tang and P.W. Bai, *J. Magn. Magn. Mater.,* 409 (2016) 39.
11. L. Tao, H. Li, J. Shen, K. Qiao, W. Wang, C. Zhou, J. Zhang and Q. Tang, *J. Magn.Magn. Mater*. 375 (2015) 124.
12. Z.Y. Cao, X.F. Ding, R. Bagheri, A. G. Wattoo, C. Xu, L.J. Yang, L.X. Song, Y.Q. Wen and Z.L. Song, *Vaccum*, 142 (2017) 37.
13. X.L. Wang, L.N. Zhao, K.H. Ding, S.L. Cui, Y. C. Sun and M.S. Li, *Chin. Phys*. B, 24 (2015) 037506
14. X.L. Wang, L.N. Zhao, K.H. Ding, S.L. Cui, Y.C. Sun and M.S. Li, *Rare Metal Mat. Eng*., 45 (2016) 309.
15. X.L. Wang, Q.X. Hu, K.H. Ding, Z.J. Peng, Y.C. Sun and M.S. Li, *J. Cent. South Univer*., 23 (2016) 2763.
16. Y.X. Qiao, Z.H. Tian, X. Cai, J. Chen, Y.X. Wang, Q.N. Song and H.B. Li, *Tribol. Lett*., 67 (2019) 1.
17. J. Strzeszewski, G.C. Hadjipanayis and A.S. Kim, *J. Appl. Phys*., 64(1988) 5568.
18. W.F. Li, H. Sepehri-Amin, T. Ohkubo, N. Hase and K. Hono, *Acta Mater*., 59( 2011) 3061.
19. T. H. Kim, S. R. Lee, M. W. Lee, T. S. Jang, J. W. Kim, Y. D. Kim and H. J. Kim, *Acta Mater*., 66

(2014) 12.
20. A.A. EI-Moneim, A. Gebert, M. Uhlemann, O. Gutfleisch and L. Schultz, *Corros. Sci*., 44 (2002) 1857.
21. F.E. Camp and A.S. Kim, *J. Appl. Phys*., 70 (1991) 6348.
22. H. Shi, Y.X. Qiao, X. Cai, J. Cui, Y.P. Chen, Y. Qin and X.Y. Wang, *Int. J. Electrochem. Sci.*, 12 (2017) 11298.
23. A. Gebert, A.A. El-Moneim, O. Gutfleisch and L. Schultz, *IEEE T Magn*., 38 (2002) 2979.
24. Z.P. Shi, Z.B. Wang, J.Q. Wang, Y.X. Qiao, H.N. Chen, T.Y. Xiong and Y.G. Zheng, *Acta Metall*. Sin. (English Letters) (2019). DOI.org/10.1007/s40195-019-00947-7.
25. Y.X. Qiao, X. Cai, C. Ouyang, Y.G. Zheng, *Int. J. Electrochem. Sci*., 11 (2016) 10329.
26. Q.N. Song, N. Xu, W. Gu, Y.F. Bao, C.Y. Wei, F.S. Ni, Y.G. Zheng, D.R. Ni and Y.X. Qiao, *Int. J. Electrochem. Sci.*, 12 (2017) 10616.
27. B. Chanita, P. Kharittha, W. Worawit, *Spectrochimica Acta* A, 224 (2020) 117351.
28. P. Zhang, L. Liang, J. Jin, Y. Zhang, X. Liu and M. Yan, *J. Alloys Compd*., 616 (2014) 345-349.